Biomicrofluidics ARTICLE scitation.org/journal/bmf

Toward embryo cryopreservation-on-a-chip: A standalone microfluidic platform for gradual loading of cryoprotectants to minimize cryoinjuries

Cite as: Biomicrofluidics **15**, 034104 (2021); doi: 10.1063/5.0047185
Submitted: 10 February 2021 · Accepted: 8 April 2021 ·
Published Online: 18 May 2021

Pouria Tirgar,[1,2] Fatemeh Sarmadi,[1,3] Mojgan Najafi,[1] Parinaz Kazemi,[1,4] Sina AzizMohseni,[1,5] Samaneh Fayazi,[1] Ghazaleh Zandi,[1] Nikta Ziaie,[1] Aida Shoushtari Zadeh Naseri,[1] Allen Ehrlicher,[2] and Mojtaba Dashtizad[1,a)]

AFFILIATIONS

[1]Embryo Biotechnology Laboratory (EmBio Lab), Department of Animal Biotechnology, National Institute of Genetic Engineering and Biotechnology (NIGEB), Tehran 1497716316, Iran
[2]Department of Bioengineering, McGill University, Montreal, Quebec H3A0B9, Canada
[3]Department of Physiology, McGill University, Montreal, Quebec H3G1Y6, Canada
[4]Department of Biology, McGill University, Montreal, Quebec H4A3J1, Canada
[5]Electrical Engineering Department, University of British Columbia, Vancouver, British Columbia V6T1Z1, Canada

[a)]**Author to whom correspondence should be addressed:** dashtizad@nigeb.ac.ir. **Tel.:** +98-21-44787323. **Fax:** +98-21-44780395

ABSTRACT

Embryo vitrification is a fundamental practice in assisted reproduction and fertility preservation. A key step of this process is replacing the internal water with cryoprotectants (CPAs) by transferring embryos from an isotonic to a hypertonic solution of CPAs. However, this applies an abrupt osmotic shock to embryos, resulting in molecular damages that have long been a source of concern. In this study, we introduce a standalone microfluidic system to automate the manual process and minimize the osmotic shock applied to embryos. This device provides the same final CPA concentrations as the manual method but with a gradual increase over time instead of sudden increases. Our system allows the introduction of the dehydrating non-permeating CPA, sucrose, from the onset of CPA-water exchange, which in turn reduced the required time of CPA loading for successful vitrification without compromising its outcomes. We compared the efficacy of our device and the conventional manual procedure by studying vitrified–warmed mouse blastocysts based on their re-expansion and hatching rates and transcription pattern of selected genes involved in endoplasmic reticulum stress, oxidative stress, heat shock, and apoptosis. While both groups of embryos showed comparable re-expansion and hatching rates, on-chip loading reduced the detrimental gene expression of cryopreservation. The device developed here allowed us to automate the CPA loading process and push the boundaries of cryopreservation by minimizing its osmotic stress, shortening the overall process, and reducing its molecular footprint.

INTRODUCTION

Since its introduction in 1983,[1] embryo cryopreservation has emerged as an attractive infertility treatment option, resulting in thousands of successful live births.[2] By suppressing the metabolism and biochemical reactions at cryogenic temperatures, cryopreservation allows for long-term storage of biological samples for future use or analysis by stopping their "biological clock." However, in practice, this process imposes a major threat to the structural integrity of the cells, that of ice crystal formation.[3] The main approaches currently used to counteract this issue are to either dehydrate the cell and remove the intracellular water or replace it with cryoprotective agents (CPAs), or both.[4,5] Since most CPAs are highly toxic for cells, initial methods used them at very low concentrations, followed by controlled and slow cooling of the sample.[6] While this

method, called slow-freezing, was the clinical standard of embryo cryopreservation for years, it greatly suffered from practical complications (e.g., the need for expensive programmable freezers, tedious process, etc.) plus the formation of intracellular ice-crystals and hence lower outcomes.[7,8] One solution to overcome the shortcomings of slow-freezing is to increase the concentration of CPAs. However, this, in turn, necessitates a rapid water-CPA exchange and an ultra-fast cooling rate, altogether comprising the current gold standard technique of cryopreservation and vitrification.[9]

Although this elevated CPA concentration can appreciably suppress ice crystal formation, it also applies high osmotic pressure on the cytoplasmic membrane during the CPA loading and unloading.[10] This osmotic shock has also been shown to cause irreversible damages to proteins,[11] the Endoplasmic Reticulum (ER), and oxidative stress-induced apoptosis.[12,13] One common practice to mitigate the impacts of this anisosmotic water-CPA exchange condition is to gradually increase the concentration of CPAs in a series of discrete steps.[14,15] This stepwise protocol is widely accepted to improve the post-warming viability and developmental competency.[16,17] However, the number of steps cannot be unlimited due to the physical restrictions of conventional manual procedures. Thus, the ideal CPA loading procedure should be practically feasible and at the same time minimize abrupt changes in osmolarity. One potentially promising approach to achieve these goals is using microfluidic systems.

With a growing range of applications, microfluidic systems have now become a successful solution for precise manipulation of fluids with micro-scale flow features such as laminar streams[18] and concentration gradients.[19,20] These properties have given microfluidic systems unique potentials for a myriad of applications in reproductive biomedicine, ranging from sperm sorting[21,22] and oocyte selection[23,24] to *in vitro* fertilization (IVF)[25,26] and embryo culture.[27,28] Despite their encouraging results, most, if not all, of these systems heavily depend on peripheral macroscopic equipment such as pumps, valves, and connections for liquid handling,[29–33] making them more of a lab-around-a-chip ensemble than the initial notion of lab-on-a-chip devices.

Interestingly, microfluidic systems were also used in cryopreservation of cells[34] and genetic resources,[35–38] though their scope has not gone further than eight-cell embryos and excluded later developmental stages of cleaved embryos. This is despite the fact that cryopreservation of fully developed preimplantation embryos (expanded blastocysts) is becoming an essential practice in assisted reproduction, given its critical role in the global trend toward single embryo transfer.[39,40] However, blastocysts are inherently vulnerable to cryopreservation, mostly due to the presence of a large volume of water in blastocysts, called blastocoel fluid, that imposes a huge barrier to water-CPA exchange.[41]

To overcome the above-mentioned challenges, here we introduce a novel microfluidic device for mouse blastocyst vitrification that offers a new set of integrated capabilities. It is a fully standalone and portable device and provides a temporal concentration gradient of CPAs, enabling simple and direct embryo loading/retrieval. This platform can significantly minimize the shrinkage rate and maintain the spherical morphology of blastocysts through a controlled and continuous CPA loading profile. Beyond cellular impact, we show that this novel approach also positively impacts the molecular footprint of vitrification on stress-related genes (*XBP-1*, *SOD1*, *SOD2*, *HSP70*, *TP53*, *Caspase 3*). Our device allows us to vitrify the embryos at a lower final concentration of CPAs and in a shorter period, all while achieving comparable results and without compromising the effectiveness of the process.

METHODS AND MATERIALS

Device fabrication

Microfluidic chips were fabricated using a standard soft-lithography process.[42,43] Briefly, we used AutoCAD to design the mask pattern that was later printed on a transparency plastic sheet. Then, as schematically shown in Fig. 1(a), a positive master mold with a thickness of 120 μm was fabricated from a flexible photomask in SU-8 2050 (MicroChem, Newton, MA) on a silicon wafer using conventional photolithography. The micropatterns were then replicated into PDMS (Sylgard 184: DOW Corning, MI) with a 1:10 (wt/wt) mixing ratio and cured in the oven at 90 °C for 1 h. Dermal biopsy punches were used to punch a 5-mm diameter outlet and two 2-mm diameter ports, one as the inlet for CPA loading and the other for a chamber where embryos will be placed and kept during the process. These ports, along with the dimensions of the rest of the chip, are shown in Fig. 1(b), where the fluid flows from the inlet at the left toward the outlet port at the right. Oxygen plasma exposure was used to render PDMS microchannels hydrophilic and bond PDMS to the glass substrate using a plasma etch unit (Denton Vacuum LLC, Moorestown, NJ) for about 30 s at 180 mTorr pressure.

Simulation of the CPA concentration profile

The fluid behavior in the microfluidic device was numerically simulated using COMSOL Multiphysics. Since changes in the concentration are—mostly—a function of mass transfer of CPA molecules, we analyzed the two main molecular bases of mass transfer in microfluidic; convection, and diffusion. Equation (1) shows the combined convection–diffusion equation that was used in this work, where the term $-\nabla.(uc)$ is an expression of convective mass transfer, $\nabla.(D\nabla c)$ describes mixing through molecular diffusion between adjacent domains, c is the solute concentration, D is the diffusion coefficient, ∇ represents gradient, $\nabla.$ represents the divergence, and u is the velocity field that the fluid is moving within,

$$\frac{\partial c}{\partial t} = \nabla.(D\nabla c) - \nabla.(uc). \tag{1}$$

The velocity field of fluid flow can be driven using the incompressible momentum Navier–Stokes equation [Eq. (2)], where u is the fluid velocity field, p is the fluid pressure, ρ is the fluid density, υ is the kinematic viscosity, and ∇^2 is the Laplacian operator,

$$\frac{\partial u}{\partial t} + u.\nabla u = -\frac{\nabla p}{\rho} + \upsilon\nabla^2 u. \tag{2}$$

To calculate the concentration changes over time, Eqs. (1) and (2) should be solved in a fully coupled approach for which we employed a COMSOL Multiphysics diluted species interface

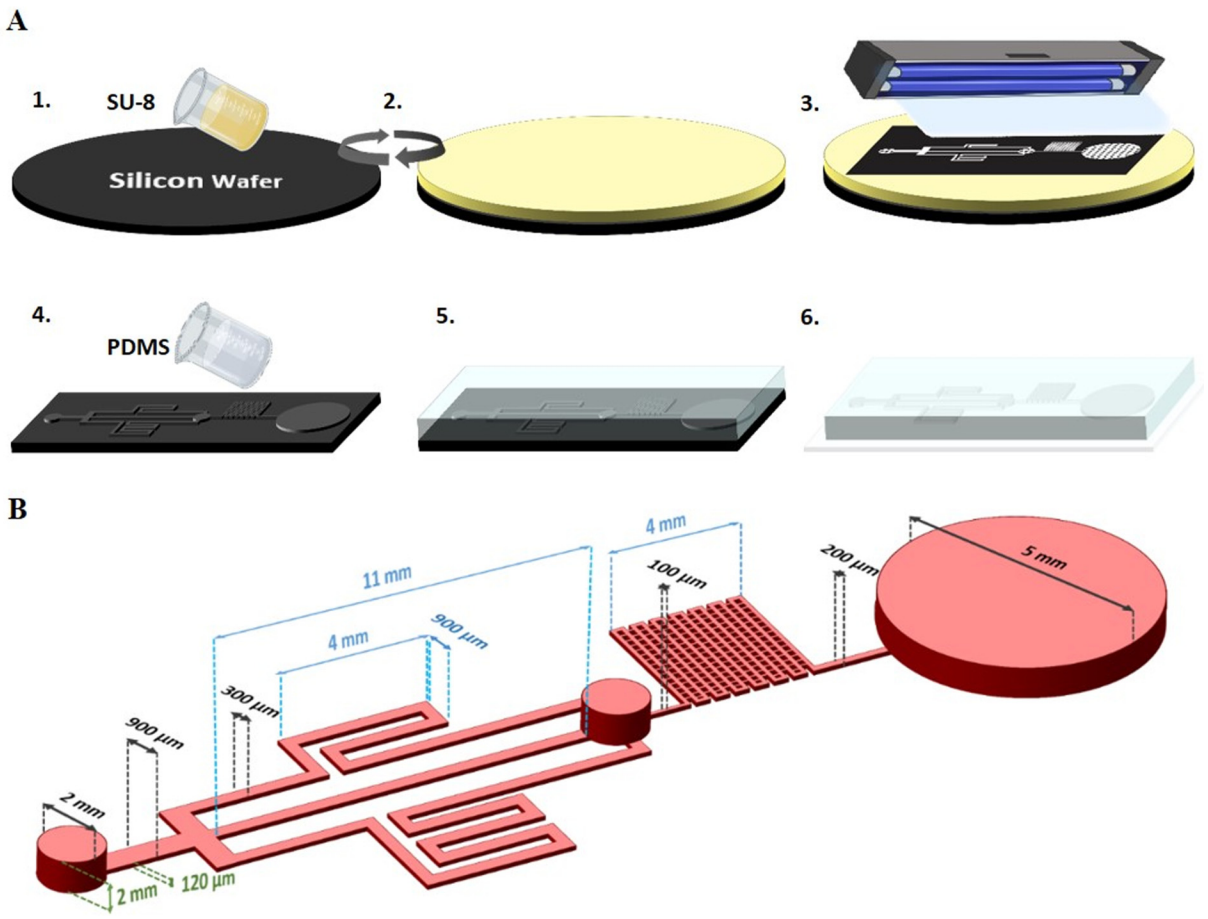

FIG. 1. (a) Schematic summary of the steps taken in the fabrication method used in this work, including photo-resist spin coating and baking, UV exposure through the mask and development (steps 1–3), replica molding in PDMS silicon (steps 4 and 5), and plasma bonding (step 6). (b) Dimensions of different parts of the microfluidic chip used in this work. The channel height (thickness) is 120 μm for all channels, and the inlet is at the left side of the schematic.

(laminar flow). The measured fluidic properties and applied boundary conditions that are used to simulate the behavior of this device are listed in Table I. The density and dynamic viscosity of the fluids were measured using a pycnometer and a viscometer (LOVIS2000, Anton Paar, Austria), respectively. We then used numerical simulation to predict and calculate the concentration of sucrose in the embryo chamber during the 900s following CPA loading.

TABLE I. Fluid properties and boundary condition values used for the numerical simulation.

Parameters	Description	Value
Base medium density	ρ_{BM}	1128 kg/m^3
Cryoprotective solution density	ρ_{cs}	1198 kg/m^3
Base medium dynamic viscosity	μ_{BM}	10.15×10^{-4} Pa s
Cryoprotective solution dynamic viscosity	μ_{cs}	15.13×10^{-4} Pa s
Sucrose molecular diffusivity	D	1×10^{-9} m^2/s
Sucrose concentration at the inlet	c	700 mol/m^3

Device characterization

To characterize the fluid flow in microchannels, the cryoprotective solution (CS) was prepared by dissolving 21% dimethylsulfoxide (DMSO) (D-2650; Sigma-Aldrich, Darmstadt, Germany), 21% ethylene glycol (EG) (324558; Sigma-Aldrich, Darmstadt, Germany), and 0.7M sucrose (S9378; Sigma-Aldrich, Darmstadt, Germany) in the base medium (BM) (HEPES-buffered tissue culture medium (12340-030; Gibco, USA) supplemented with 20% fetal bovine serum (10270; Gibco, USA). Then, 5 mg/ml of Rhodamine B (R6626; Sigma-Aldrich, Darmstadt, Germany) was dissolved in the CS. Images and videos of the fluid flow were captured on an inverted fluorescent microscope (Nikon Ti, Japan). To characterize the

temporal concentration gradient in the embryo chamber, we used a 5.2 mM solution of a marker dye, Brilliant Cresyl Blue ALD (B5388; Sigma-Aldrich, Darmstadt, Germany) with a close molecular weight (MW: 385.9 g/mol) to sucrose (MW:342.3 g/mol) in the CS. We then quantified the absorbance of a serial dilution of this media at 682 nm using a UV–Vis spectrophotometer (Specord 200; Analytik Jena, USA) and used the Beer–Lambert law to generate a standard absorption curve of the analyte concentration (Fig. S1 in the supplementary material). To determine the solute concentration profile in the microfluidic chip, the device was filled with the BM, followed by the introduction of the dye-containing CS. Samples were collected from the embryo chamber at different time points (2, 5, 8, 10, 13, and 15 min) and their respective concentrations were calculated.

Embryo collection

All experiments involving mice were carried out in accordance with Protocol IR.NIGEB.EC.1394.8.10.A, approved by the Institutional Animal Care and Use Committee of the National Institute of Genetic Engineering and Biotechnology of Iran.

Female Naval Medical Research Institute (NMRI) mice, 6–8 weeks old, were superovulated by intraperitoneal injections of 7 IU equine chorionic gonadotropin (eCG) (Folligon, Intervet, Spain) and then 7 IU human chorionic gonadotropin (hCG) (Pregnyl, Daroupakhsh, Iran) 48 h later. Superovulated female mice were then placed overnight with the same strain males with proven fertility. The success of mating was confirmed on the next morning by the presence of a vaginal plug; the date of plug detection was considered to be embryonic day 0.5. Pregnant mice were sacrificed by cervical dislocation at the fourth embryonic day, and blastocysts were collected by flushing the uterine horns with HEPES-buffered M2 medium (M7167; Sigma-Aldrich, Darmstadt, Germany). Finally, morphologically normal expanded blastocysts were selected and kept at 37 °C in a 5% CO_2 in a humidified incubator before being used in the vitrification processes.

Manual and automated vitrification of blastocysts

Expanded blastocysts were manually vitrified using Cryotop (Kitazato, Japan), as described by Kuwayama[44] with slight modifications. Briefly, blastocysts were gently washed in the BM. Then, embryos were transferred to and kept in the equilibration solution (ES) consisting of 7.5% EG and 7.5% DMSO in the BM at room temperature (22–25 °C) for 15 min. Following equilibration, embryos were rinsed four times in small droplets of vitrification solution (VS) consisting of 15% DMSO, 15% EG, and 0.5 M sucrose in the BM within 45–60 s. Subsequently, shrunken embryos were loaded on Cryotops and quickly plunged into liquid nitrogen (LN_2) for storage.

In automated vitrification, the microfluidic device was filled with the BM, and expanded blastocysts were placed into the embryo chamber. Then, the CS was loaded in a standard 200 μl micropipette tip, which had been previously slid in the inlet port of the chip. To create a flow direction toward the embryo chamber, hydrostatic pressure was generated by the height of CS. Following exposure to the increasing concentration of CPAs, blastocysts were removed from the chip at specific time points, loaded onto a Cryotop and immediately immersed in LN_2.

Warming procedure

The Cryotop was removed from the LN_2 and immersed directly into the thawing solution (1 M sucrose dissolved in the BM) at 37 °C for 1 min, after which they were transferred to dilution solution (0.5 M sucrose dissolved in BM) for 3 min, and then into the BM for 10 min to rehydrate properly. Finally, vitrified–warmed blastocysts were cultured in a potassium simplex optimized medium (KSOM) (MR-121-D; Millipore, Darmstadt, Germany) overlaid with mineral oil (M5310; Sigma-Aldrich, Darmstadt, Germany) under the conditions described earlier. Blastocyst morphology was evaluated prior to vitrification, upon warming, and after that using a TI-U microscope (Nikon, Japan), and high-quality blastocysts were selected based on a previously established method.[45] Cryosurvival rate was defined as the percentage of re-expanded blastocysts on warming. Re-expansion and hatching rates were monitored 12 h post warming.

Blastocyst morphological analysis, shrinkage, and sphericity

To study the morphological impacts of CPA loading on embryos, embryos were monitored throughout the CPA loading process in both the microfluidic setup and when transferred between droplets in the manual process, using a monochromic camera on a Nikon TE2000-U inverted microscope. The diameter of the blastocysts was then measured using ImageJ and used to calculate the volume of the embryo assuming an ideal spherical geometry.

RNA isolation and real-time qPCR

Total RNA was extracted from 200 blastocysts of each group using an RNase Plus Micro Kit (74034; Qiagen, Valencia, CA), in accordance with the manufacturer's protocol. cDNA was synthesized by an AccuPower® RocketScript™ RT PreMix kit (Bioneer, Korea) using random hexamer primers. The qPCR reaction was prepared at a final volume of 10 μl by mixing 5 μl of 2× SYBR Green PCR Master Mix (25344; Intron, Korea), 2 μl of cDNA, and 0.2 μM of each primer (Table SI in the supplementary material). Real-time PCR was carried out with a Mic qPCR Cycler (Bio Molecular Systems, Australia) under following thermal conditions: 95 °C for 5 min, 45 cycles of 95 °C for 15 s, 61 °C for 15 s, and 72 °C for 15 s. Melting curves were analyzed after 45 cycles to confirm the specificity of PCR products. Relative Expression Software Tool (REST) was used to determine the relative transcript abundance of desired genes, using β-actin as the reference gene.

Experimental design

The experiments are conducted in three main steps (Fig. 2): (a) determining the concentration profile of a cryoprotective solution over time in the microfluidic system (b) finding the optimum time–concentration condition for the microfluidic-based CPA loading in comparison with the manual method, and (c) comparing the molecular impact of this selected on-chip condition with the traditional droplet-based method. In the initial step (a), we first created a serial dilution of dye-containing CS and used spectrophotometry to generate an absorbance–concentration standard curve based on the Beer–Lambert law. We then validated our simulation results by measuring the CS concentration in the chip over time based on absorbance

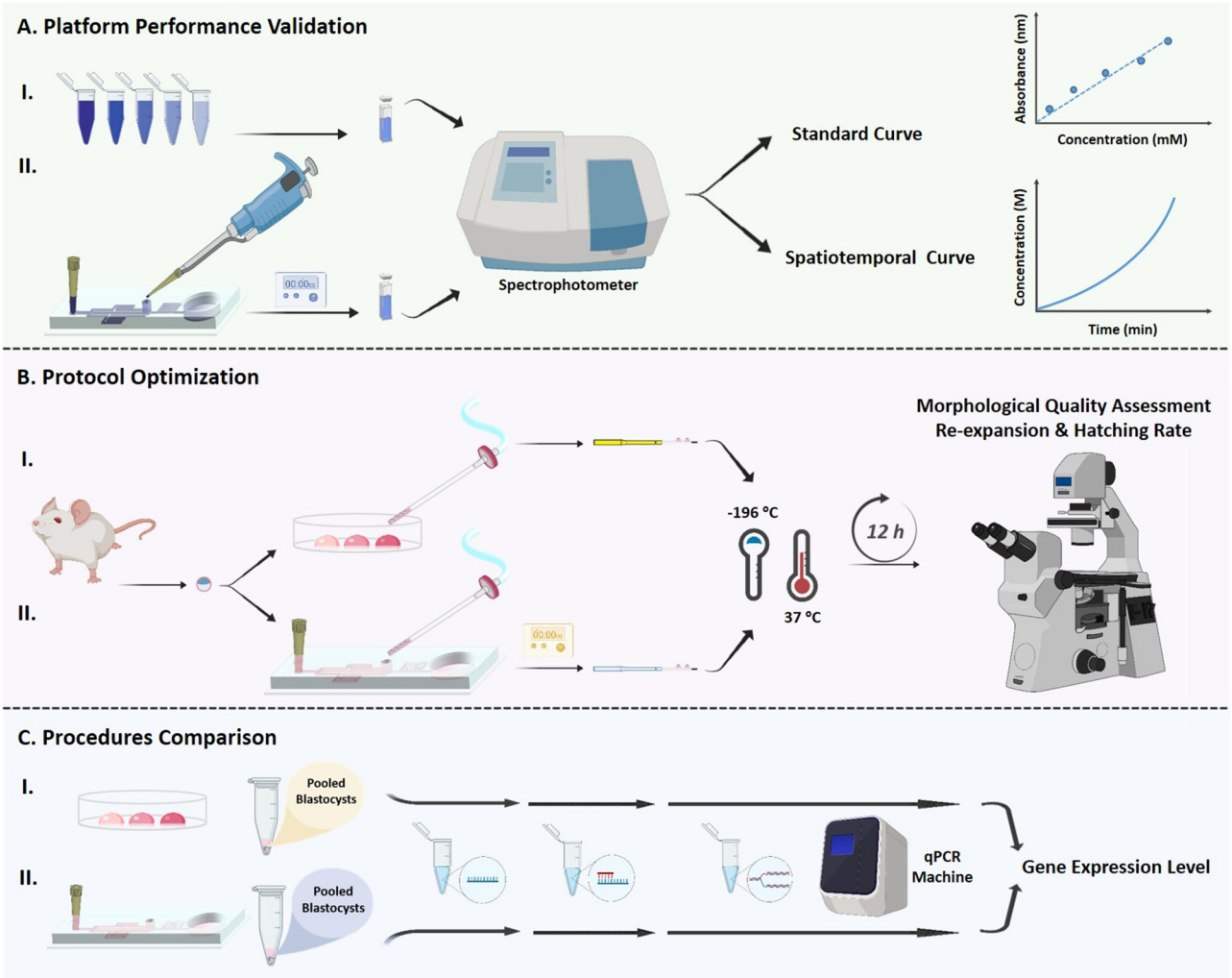

FIG. 2. General representation of the experimental design. (a) A standard curve was generated (A I) by making a serial dilution of the marker dye and measuring the absorbance of each sample with a spectrophotometer. This curve along with the Beer–Lambert law was then (A II) used to measure the concentration of CS in the chip over time from samples taken at different time points. (b) Embryos were vitrified–warmed using either the manual method (B I) or different conditions (time–concentration) of the on-chip system (B II). Embryos were evaluated 12 h post warming for their morphology, re-expansion, and hatching rates to select the optimum on-chip condition. (c) The gold standard manual protocol (C I) was analyzed against the optimum on-chip (C II) condition based on the expression pattern of selected genes (qRT-PCR) in blastocysts vitrified–warmed with both techniques.

values and the standard curve generated earlier. In the second stage (b), *in vivo* produced blastocysts were randomly divided into five groups and transferred into the embryo chamber for CPA loading. Embryos were then exposed to the CPA solution for different time lengths (6, 9, 12, 15, and 18 min) and then transferred to liquid nitrogen for vitrification. Upon warming and after 12 h, we evaluated the re-expansion and hatching rates of these blastocysts and compared them to the manual method to determine the most favorable on-chip cryoprocedure. In the third stage (c), embryos vitrified–warmed by this optimum on-chip condition were compared to their counterparts from the manual vitrification process based on the transcription pattern of selected genes.

STATISTICAL ANALYSIS

All experiments were repeated at least three times, and results are expressed as means ± SD. A student's *t*-test was used for comparison of two groups. The SPSS 16.0 software was used for this analysis, and a P value of <0.05 was considered statistically significant.

RESULTS

Device architecture and operation

Here, we designed and fabricated a microfluidic chip that can expose blastocysts to an automatic, constant, and gradual increase

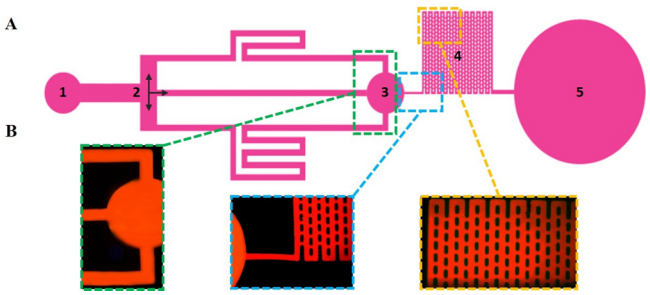

FIG. 3. (a) Schematic design of the microfluidic chip, comprised five main sections: inlet (1), CS delivering microchannels (2), embryo chamber (3), capillary pump (4), and outlet (5). (b) Fluorescent images of different parts of the device filled with CS containing Rhodamine B.

in CPA concentration. By avoiding abrupt changes in the solute concentration, this system can minimize the osmotic pressure on the embryo during the CPA loading process. The chip is comprised of five main sections: inlet reservoir, CS delivering microchannels, embryo chamber, capillary pump, and the outlet [Fig. 3(a)]. To simplify the operation, this pumpless system uses the hydrostatic pressure difference between the inlet and the embryo chamber to drive the fluid flow inside the microchannels. The inlet is connected to the embryo chamber through three microchannels with different lengths and hence different resistances and fluid flow in the channels. Thus, after filling the chip with BM and loading the CS in the inlet reservoir, CS will reach the embryo chamber in three steps, with each one gradually adding more CPAs to the chamber. The outlet of the chamber is connected to a capillary pump [Figs. 3(a)–3(b)] that serves two main purposes, facilitating the initial flow of BM in the chip and controlling the chamber outflow by acting as a flow resistor during operation.

Cryoprotectant concentration profile in the chip

We used numerical simulation to gain a quantitative prediction of the flow behavior and concentration changes in our microfluidic system. We selected sucrose, one of the CPAs in the CS, as a candidate and numerically simulated its concentration over time in the embryo chamber for different hydrostatic pressure values (data not shown). We found that 82.5 Pa of pressure (~7 mm in height) in the inlet results in the same ultimate concentration as in the manual procedure at the end of the 15-min loading time. Figure 4(a) shows the snapshots of this simulation at different time points. Given the design of the chip, each of the three main CS delivering channels imposes a different resistance (channel length) to the fluid flow,

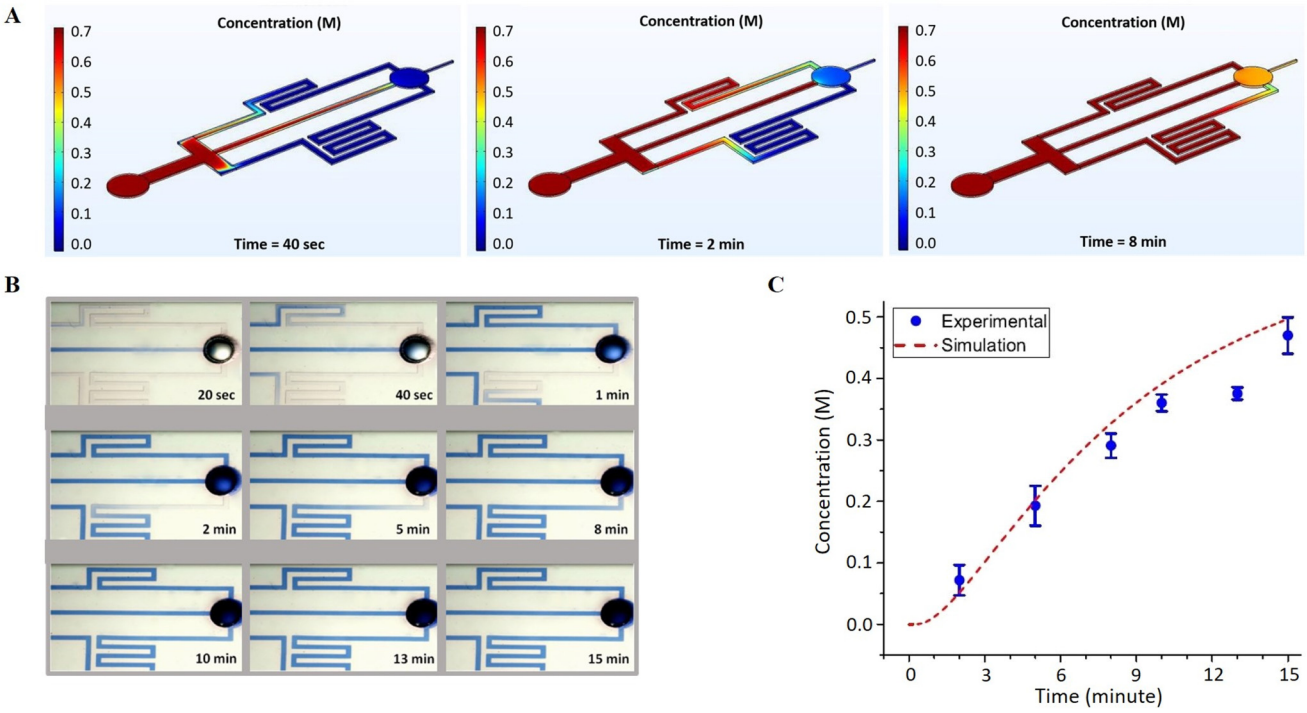

FIG. 4. Theoretical and experimental CPA concentration changes over time (a) Numerical simulation of the sucrose concentration in the embryo chamber at different time points for 82.5 Pa hydrostatic pressure at the inlet (~7 mm height of CS). (b) The flow of CPAs in microchannels at different time points, visualizing the gradual concentration increase in channels and the embryo chamber. (c) Overlay of the numerically predicted sucrose concentration and the experimentally measured concentration of the marker dye in the embryo chamber of the microfluidic device over time.

creating a delay for the arrival of the CS from each channel. Using a marker dye with similar molecular weight (385.9 g/mol) to sucrose (342.3 g/mol), this gradual concentration increases in channels and consequently in the embryo chamber can be visualized as a color transition from transparent to dark blue [Fig. 4(b)]. We then quantified this concentration increase over time and compared it with the output of the numerical simulation by reading the absorbance of samples collected from the embryo chamber at multiple time points [Fig. 4(c)]. The numerical simulation and the experimentally measured dye concentration were shown to be in close agreement over 15 min and follow a gradual profile toward the expected final values.

We then compared the manual and microfluidic methods regarding their solute concentration increase over time (Fig. 5). In the manual process, the concentration increase occurs in two abrupt steps: when the embryos are moved from BM (no CPA) to ES (1.06 M DMSO and 1.34 M EG) and from ES to VS (0.5 M sucrose, 2.1 M DMSO, and 2.7 M EG), as shown in Fig 5(a). Assuming the CPA solution maintains a constant relative ratio of all three components over time (1:4.2:5.4 of sucrose:DMSO:EG), the concentration of DMSO and EG was calculated relative to that of sucrose for any time point [Fig. 5(b)]. This concentration profile shows that unlike the manual method, the microfluidic system provides a smooth gradual concentration increase over time while providing the same final CPA concentration (0.5 M sucrose, 2.1 M DMSO, and 2.7 M EG). This similar ultimate condition leaves the CPA concentration profile as the only variable between the two methods, enabling their direct comparison.

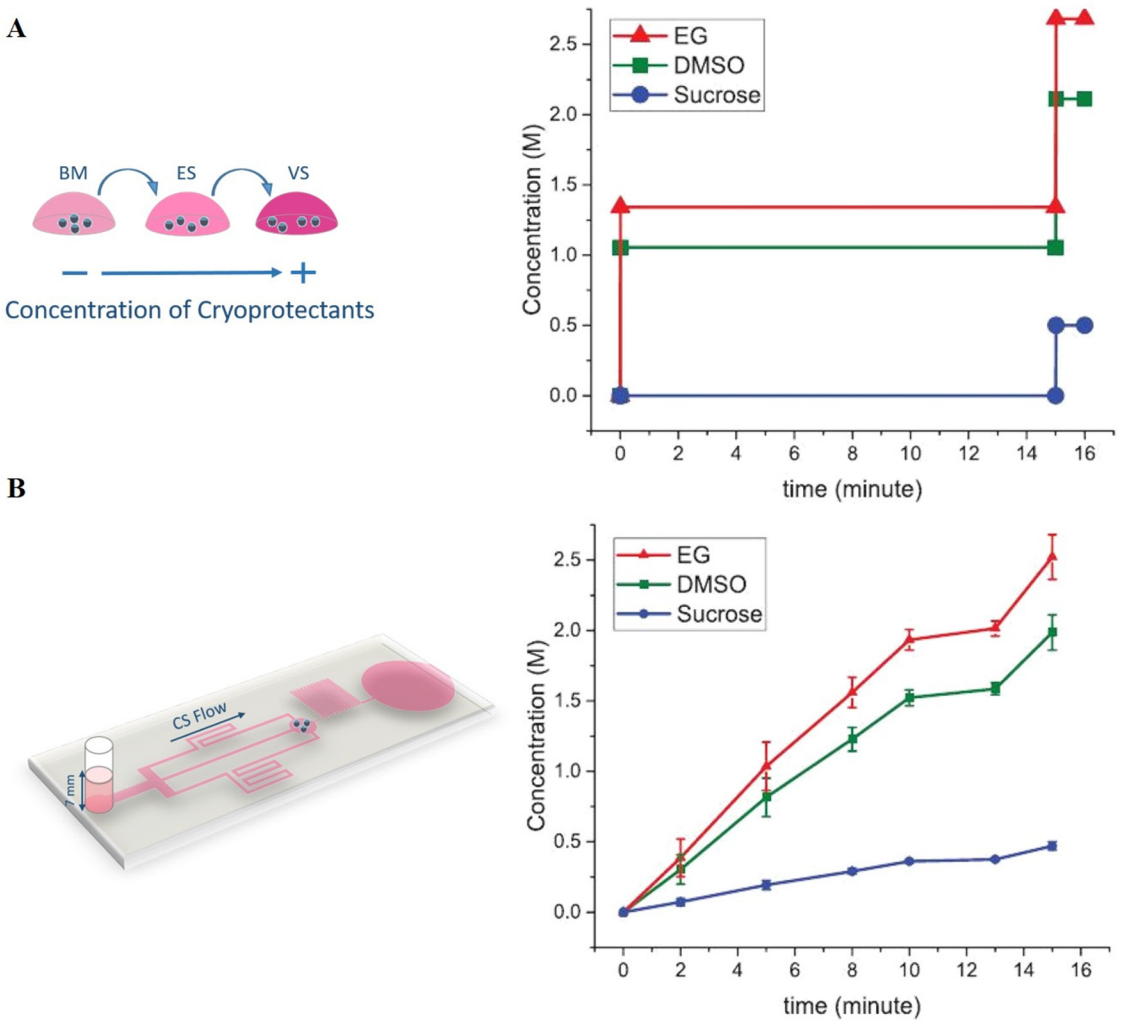

FIG. 5. Comparison of the CPA concentration profile in the manual and on-chip CPA loading protocols. (a) Schematic representation of the embryo transfer between droplets in the manual method and the corresponding sudden concentration increase of permeating and non-permeating CPAs in each step. (b) Schematic drawing of blastocysts in the microfluidic chip and the gradually increasing concentration profile of CPAs in the embryo chamber over 15 min, from 0 to 0.5 M for sucrose and proportionally for the other two CPAs.

Blastocyst cryosurvival and morphology

Given that the CPA concentration is directly proportional to the CPA loading time and hence they change together in the microfluidic device, we first decided to find the optimum point of this time–concentration profile where the re-expansion and hatching rates are the highest. As expected, the lower end of the time–concentration spectrum, which represents loading less CPA over a short period of time (6 and 9 min), resulted in poor re-expansion rates of 86.61% and 87.03%, respectively. Increasing the CPA loading time to 18 min showed the same effect by bringing down the re-expansion rate of blastocysts to 84.06%. Interestingly, unlike the manual control group with the post-warming re-expansion rate of 97.40%, on-chip loading of CPAs over the same time-span resulted in a rate as low as 83.35%. However, reducing the exposure time to 12 min for the microfluidic group significantly improved the re-expansion of blastocysts to (96.07%), which is comparable to the control group (97.4%) and implies the importance of the loading profile compared to the final concentration of CPAs (Table II).

One fundamental difference between the droplet and on-chip CPA loading methods is the rate of the morphological changes of the embryos throughout the process. In the first step of the manual method, the equilibration step, embryos are exposed to a low concentration of CPAs (i.e., the ES solution) for a long period of time. While blastocysts show minor (less than 20%) calculated volume changes in this stage, they later experience an abrupt increase of the CPA concentration in VS, causing a severe volume excursion (64%) over 1 min [Fig. 6(a)]. However, continuous exposure to the CS in the microfluidic device results in a constant but gradual water-CPA exchange that minimizes the sudden shrinkage of embryos and distributes it over the whole process [Fig. 6(a)]. This difference in the loading profiles, in turn, caused a striking difference between the manual and on-chip methods in terms of post-CPA loading morphology of blastocysts. Unlike severely collapsed embryos from the manual method, the blastocysts maintained their initial spherical morphology during the on-chip process, indicating that there is reduced CS-imposed mechanical stress in the microfluidic device [Fig. 6(b)] (Multimedia view). This geometry preservation during the volume reduction can be due to the gradual CPA increase on the chip, which spreads the exchange of water molecules with CPAs over a longer period and prevents sudden morphological changes.

TABLE II. The effect of CPA loading time on re-expansion and hatching rates of vitrified–warmed blastocysts in the microfluidic approach and the manual method. Values with superscripts a–c are significantly different (mean ± SD, $P < 0.05$).

Groups		Re-expansion rate (%)	Hatching rate (%)
Manual CPA loading		$97.40^{a} \pm 1.53$	$44.40^{a} \pm 5.69$
On-chip CPA loading	6 min	$86.61^{b} \pm 3.25$	$22.73^{b} \pm 1.90$
	9 min	$87.03^{b} \pm 3.78$	$26.18^{b} \pm 3.05$
	12 min	$96.07^{a} \pm 1.88$	$38.80^{a} \pm 1.02$
	15 min	$83.35^{b} \pm 2.17$	$25.52^{b} \pm 3.34$
	18 min	$84.06^{b} \pm 3.08$	$17.01^{c} \pm 0.85$

Molecular responses to manual and on-chip CPA loading profiles

To further analyze the impact of the on-chip CS exposure on embryos, vitrified–warmed blastocysts from both manual and microfluidic methods were compared at the molecular level. We examined the transcription profile of six genes related to endoplasmic reticulum stress (XBP1), oxidative stress (Sod1 and Sod2), heat shock (Hspa1a), and apoptosis (Trp53 and Caspase 3). As shown in Fig. 7, using the microfluidic system resulted in a 40% decrease in expression of the ER stress-related gene XBP1. Moreover, on-chip CPA loading significantly downregulated the expression level of Sod1 and Sod2 (0.6 and 0.8, respectively), though Hspa1a was equally transcribed in both groups. Similarly, there has been no significant difference in transcript abundance of Trp53, while the other apoptosis candidate gene, Caspase 3, was considerably downregulated in the blastocysts vitrified with a microfluidic device.

DISCUSSION

In this work, we introduced a novel microfluidic system for mouse embryo vitrification to minimize the osmotic shock to embryos by generating a gradual and controlled CPA loading profile. The well-explored potential of microfluidic systems in creating highly controllable concentration gradients was previously used in a wide range of applications, from droplet generation[46] to chemotaxis studies,[47,48] and even CPA loading of somatic[49,50] and germ cells.[51,52] However, these CPA loading platforms failed to address two major challenges associated with the benchtop use of microfluidic for CPA loading. First, minimizing the cytotoxicity of CPAs requires the loading process to be immediately followed by the cooling step (i.e., transferring the sample to liquid nitrogen). Often composed of fully sealed microchannels, traditionally enclosed systems make it nearly impossible to load or retrieve samples at exact time points or necessitate complex systems such as valves[37] or vacuum pumps.[53] Second, while these chips make it "easier" to control the CPA concentration pattern on the chip, this "ease" has mostly come at the price of adding an array of equipment (i.e., programmable pumps) to the system that in turn complicate its operation and undermine the main incentive for using microfluidic for CPA loading. The system proposed in this work is, to the best of our knowledge, the first openly accessible and pumpless microfluidic chip for cryopreservation that allows samples to be directly loaded in the chip, be exposed to a controlled CPA gradient, retrieved with direct access, and vitrified immediately after. Such properties will allow researchers and technicians to use this new system with small to no changes to their setup and also makes this chip a portable solution for remote areas that lack equipment and experienced personnel.

Besides commonly referenced advantages of using microfluidic systems for biological applications (e.g., faster reaction and lower reagent consumption), the presence of the fluid flow (vs a static droplet) is an extra practical advantage for applications that involve sample loading /unloading. Here, the fluid flow toward the capillary pump guides embryos toward the outlet of the embryo chamber, making it easier to (re)locate and collect them after the procedure and offers a sample-loss-free pipeline. This is a huge advantage

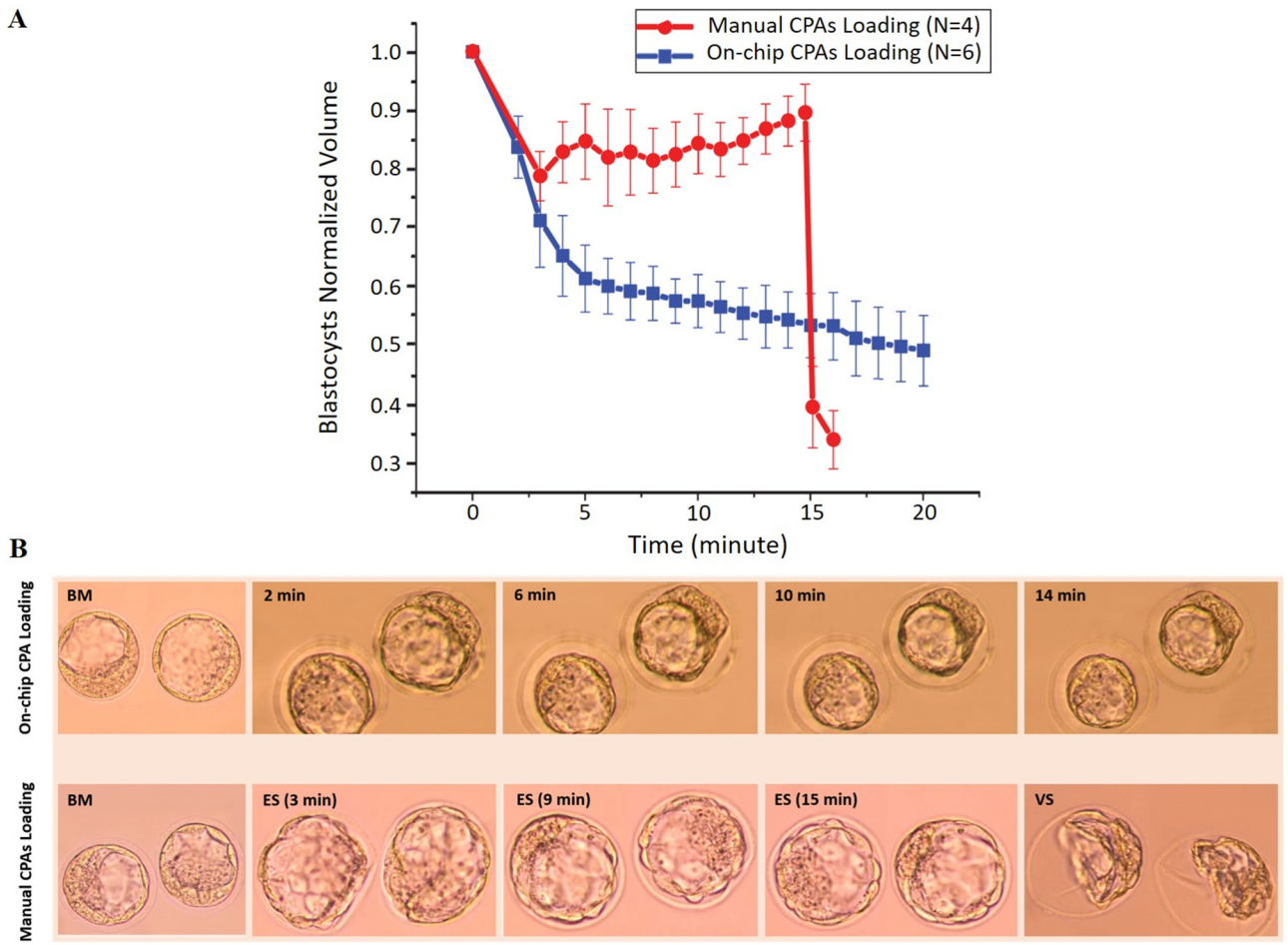

FIG. 6. Morphological changes of blastocysts during a full CPA loading process using the manual and on-chip methods. (a) Normalized calculated volume of blastocysts during CPA loading in the droplet-based and microfluidic approach. Sudden introduction of the VS solution in the manual process caused a drastic volume reduction, a transition that occurred gradually using the on-chip protocol. (b) Brightfield images of embryos during CPA loading and their morphological changes over time. Multimedia view: https://doi.org/10.1063/5.0047185.1

over the conventional protocol, where embryos are transferred to multiple droplets with sequentially increasing CPA fractions for manual creation of a concentration gradient. This is not only labor-intensive and time-consuming, but transferring embryos to and from multiple viscous and large droplets (millimeter-sized droplets vs ~0.1 mm diameter blastocysts) can lead to loss of some embryos during these transfers, losing invaluable genetic materials.

In this on-chip CPA loading protocol, embryos are exposed to a continuous and gradual CPA concentration increase instead of stepwise and sudden jumps in the traditional method (Fig. 5). Heo *et al.* previously showed that this smoothening of the loading profile is directly related to the rate of oocyte volumetric changes.[37] They found that loading a permeating CPA with a gradual profile resulted in a volumetric shrinkage rate as low as 0.005% per second (s^{-1}) compared to the 0.7% s^{-1} shrinkage rate caused by the stepwise CPA loading. More recently, Guo *et al.* showed that this high shrinkage rate causes further downstream osmotic stress injuries in oocytes.[51] In their experiments, excluding both cooling and warming steps, oocytes that only underwent loading and unloading of, again a permeating CPA, experienced a significantly lower shrinkage rate (~0.09% s^{-1} vs ~1.4% s^{-1}) and subsequently superior developmental properties compared to their counterparts from one-step manual CPA loading. Since these two works solely focused on the CPA loading phenomenon and did not follow it up with the vitrification stage (cooling the sample), they could afford to simplify their CPA solution by leaving out an important component of most embryo vitrification solutions, non-permeating CPAs. By applying osmotic pressure to the membrane, non-permeating CPAs (e.g., sucrose) remove the intracellular water and reduce cryodamages during cooling and warming.[4] Thus, unsurprisingly, when a non-permeating

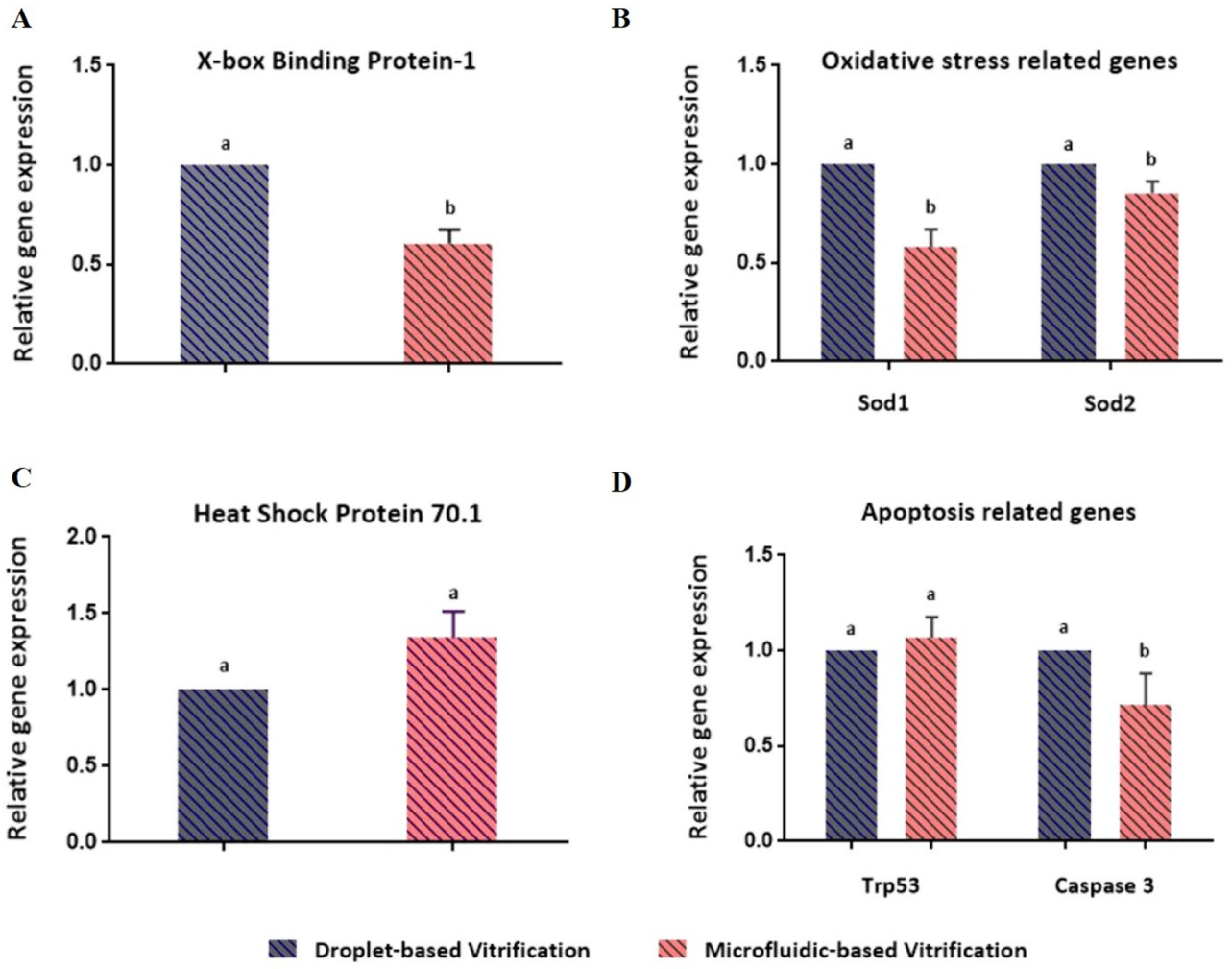

FIG. 7. The relative expression level of selected genes related to (a) endoplasmic reticulum stress (XBP1), (b) oxidative stress (Sod1 and Sod2), (c) heat shock (Hspa1a), and (d) apoptosis (Trp53 and Caspase 3). The transcription levels of XBP1, Sod1, and Sod2 were reduced when manual CPA loading was replaced by the microfluidic system, while *Hspa1a* and *Trp53* showed a similar transcription pattern in both cases, unlike Caspase 3, which was also less transcribed in the microfluidic system. Values with superscripts a and b are significantly different (mean ± SD, $P < 0.05$).

CPA is added to the solution, the shrinkage rate increases significantly. Traditionally, embryos are first exposed to only permeating CPAs for a long period of time (equilibration) and then quickly dehydrated in a solution containing non-permeating CPAs right before the cooling step, where they shrink rapidly and non-isotonically.[54] Lai *et al.* reported that this sudden introduction of impermeable CPAs results in shrinkage rates as high as 4.13% and 7.51% s^{-1} for zygotes that have or have not gone through the equilibration stage, respectively.[53] However, when they used a microfluidic chip to expose zygotes to a gradual increase of CPAs and minimize sudden changes in the osmotic pressure, the shrinkage rate was reduced down to 0.35% s^{-1}. Similarly, when we manually exposed embryos to the same equilibrium and vitrification solutions, containing both permeable and non-permeable (sucrose) CPAs, the maximum shrinkage rate was as high as 5% s^{-1}. Interestingly, this rate was reduced to 0.125% s^{-1} when CPAs were gradually loaded on the chip. Compared to the work by Lai *et al.*, the CPA loading has a lower concentration increase rate and thus takes longer to achieve the same final concentration (15 min vs 10 min total loading time); therefore, embryos experienced slower osmotic stress application and hence exhibited a lower shrinkage rate. This reduced and gradual shrinkage allows our device to introduce the non-permeating CPA (sucrose) from the beginning of the process, a condition that would impose a lethal osmotic shock to embryos if applied in the manual method due to its high osmotic stress. This early introduction of the non-permeating CPA means that embryo

dehydration can occur over the whole duration of the process (more than 14 min), instead of the short time-span of the conventional method (less than 1 min), enhancing the opportunity for improved water-CPA exchange.

The reduction of the osmotic shock and shrinkage rate extends the range of possible CPA concentrations and loading time to values that were previously osmotically lethal and hence never studied for embryo cryopreservation. We hypothesized that these new conditions can potentially be more effective than the conditions studied so far, which are limited by the lethal shrinkage rate of the manual procedure. However, there are two other critical and conflicting limitations of embryo vitrification that should be noted in evaluating new conditions. First, as schematically shown in Fig. 8, CPAs are toxic when used at high concentrations and/or for a long time (above the red solid line).[55,56] Second, for any given CPA concentration, the loading time should be long enough to allow for sufficient water-CPA exchange and successful vitrification (above the dashed curve) instead of ice crystal formation (below the curve).[57] This leaves us with a portion of the concentration–loading time plot that can minimize the side effects of cryoinjuries (hatched area). To find the conditions that fall in this category, we selected five time-concentration combinations for CPA loading (schematically represented by points 1–5 in Fig. 8). We then evaluated the viability of embryos vitrified–warmed after going through these conditions. As shown in Table II, embryos in the first two groups (6 and 9 min total CPA loading) showed significantly lower post-warming viability compared to the manual control group. Since these blastocysts were exposed to a relatively low final CPA concentration for a short period of time, their compromised viability can be due to insufficient dehydration and unsuccessful vitrification (Points 1 and 2 on Fig. 8). The third condition, where the CPA loading process was 12 min in total, appears to be the optimal condition with a viability rate as high as the manual control group. However, further increase of the final CPA concentration and loading time (to 15 and 18 min) substantially reduced the viability. This can be caused by the CPA toxicity, as discussed earlier, and shown in Fig. 8 (points 4 and 5). It is noteworthy that the 12-min condition resulted in the same cellular outcome as the manual protocol while reduced the CPA loading time by almost 3 min. This shows that, if done properly, CPA loading can happen faster without compromising the outcome. Shortening the CPA loading time has long been a goal in cryopreservation to reduce the side effects of exposing living cells to chemical CPAs. However, reducing the CPA loading time is not possible in the manual method as it generates a lethal level of osmotic stress, which became possible in the on-chip platform through its gradient concentration increase and reduced osmotic pressure.

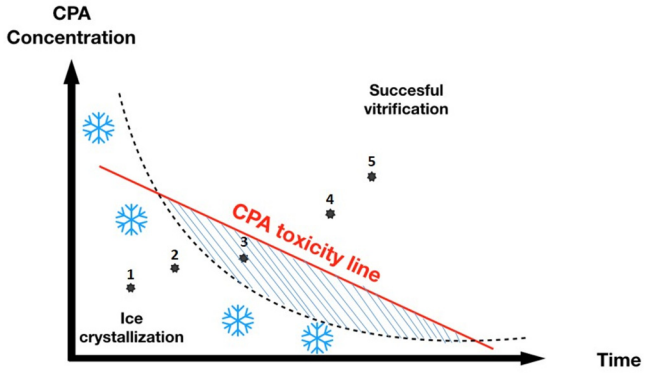

FIG. 8. Schematic representation of thermodynamics and cytotoxicity limitations of CPA loading for cryopreservation and their loading profile. The dashed curve shows the minimum CPA concentration for each loading time that prevents ice crystal formation. The solid line represents the maximum time length that embryos can be exposed to each CPA concentration. Therefore, an ideal CPA loading process should fall into the space between the dashed curve and the solid line. Points 1–5 are hypothetical representatives of the five conditions chosen for this work.

Considering the re-expansion rate (viability) as the most important parameter in embryo cryopreservation, we picked the 12-min condition as the best "on-chip" vitrified group for further analysis. We first compared their developmental competency with the manual control group, where they both showed equally high post-warming hatching rates (Table II). However, sublethal impacts of cryopreservation go far beyond the hatching rate, including its proven immediate and long-lasting molecular footprints.

As a major known source of external stress in vitrification, osmotic stress is known to induce protein structural damage and misfolding.[58,59] As schematically shown in Fig. S2 of the supplementary material, accumulation of misfolded/unfolded proteins triggers stress-response pathways, two of them shown here, as attempts to mitigate the negative impacts of the damage.[60,61] However, if the damage is beyond the capacity of the cell's repair mechanisms, the cells induce apoptosis. Since our proposed on-chip vitrification system minimized the osmotic stress applied to embryos, we expected it to also reduce the molecular impact of these osmo-responsive stress cascades. Thus, we evaluated the expression pattern of selected genes of each group and compared them in the manual (droplet) and on-chip vitrified groups.

Originally named after their heat-stress-induced upregulation, heat shock proteins or HSPs are directly involved in the handling of damaged and misfolded proteins.[62] A central component of this family of chaperons is the Hsp70.1 protein (*Hspa1a* gene), which prevents protein aggregation through transient interactions by exposed hydrophobic residues of damaged proteins.[63] Since the cryopreservation process increases the number of damaged proteins, it is not surprising that Hsp70 is reported to be overexpressed in vitrified–warmed embryos.[64] While our new on-chip technique does not modify the cooling/warming stages and CPA composition, it does change the CPA loading method. If the on-chip CPA loading reduces the efficiency of cryoprotectants by any means, it should increase the damage to proteins and hence upregulate HSP70.1. As shown in Fig. 7(c), the transcription pattern of *Hsp70.1* in the control droplet group and the microfluidic group has no significant difference, showing that the proposed on-chip protocol can be as effective as the traditional method in loading CPAs while exposing embryos to less osmotic stress. However, the impact of misfolded proteins goes beyond expression modification of chaperons and affects other subcellular components too, including organelles like Endoplasmic Reticulum (ER).

As the main folding and modification site for most proteins, ER has a distinct sense-and-response mechanism to the accumulation of damaged proteins, named Unfolded Protein Response or UPR.[65] Along with multiple other stimuli, osmotic stress is shown to disrupt ER homeostasis and promote the accumulation of unfolded/misfolded proteins within the ER lumen. This polypeptide aggregation boosts the UPR and activates the localization of its ER-to-nucleus signaling molecules. One of the main members of this family of signaling proteins is X-box binding protein 1 (XBP1), a transcription factor that activates expression of multiple stress-responsive genes, including XBP1 itself.[66,67] Here, as shown in Fig. 7(a), we observed a significant decrease in *XBP1* mRNA abundance when embryos went through the on-chip process compared to the manual droplet-based method. This implies that the on-chip CPA loading caused less ER stress and consequently did not amplify UPR rescue mechanisms, including an increase in the *XBP1* mRNA level. Another well-known effect of ER-stress is the increase in mitochondrial calcium content, which alters the metabolism and consequently elevates the level of Reactive Oxygen Species (ROS).[68] ROS are free radicals such as superoxide anions that are mostly produced as by-products of oxidation-reduction (redox) metabolic reactions in mitochondria and act as signaling molecules at low concentrations. However, excessive intracellular ROS and its subsequent oxidative stress can cause damages to the DNA and profound changes to the transcriptome. To avoid such damages, the antioxidant system of cells acts as a protective mechanism against excessive ROS accumulation to keep their concentration at the desired level.[69] The first line of defense within this system is where superoxide anions are transformed into less reactive hydrogen peroxide by two enzymes, SOD1 and SOD2, cytosolic, and mitochondrial superoxide dismutases, respectively. It is shown that the osmotic stress of hypertonic conditions promotes excessive ROS production, which in turn is known to upregulate the expression of *SOD1* and *SOD2*.[70,71] As shown in Fig. 7(b), the expression level of both *SOD1* and *SOD2* transcripts is significantly reduced when embryos went through the on-chip CPA loading process compared to those in the droplet control group. This lower transcript abundance is an indication that embryos experienced less mitochondrial stress in the microfluidic system, which excluded the need for the upregulation of antioxidant enzymes.

As mentioned before as a comprehensive consequence of elevated (extra)cellular stresses, apoptosis is proposed as one of the main reasons for post-vitrification embryo degradation.[72] Also known as type I cell death, apoptosis is a gene controlled and autonomous programmed cell death process that can be initiated by multiple mechanisms. The most common one among vertebrates is the intrinsic pathway or mitochondrial mechanism, in which pro-apoptotic signaling molecules are released upon damage to the mitochondrial outer membrane.[73] Since the on-chip CPA loading platform significantly lowered the mitochondrial damage, we expected to see its molecular impacts in the mitochondrial pathway of apoptosis too. Therefore, we looked into the relative transcription of two key genes in this pathway, tumor suppressor P53 (*Trp53*) and mitochondrial executioner caspase-3 (*CASP3*). P53 is a tumor suppressor transcription factor that regulates the expression of dozens of genes involved in multiple pathways from DNA repair and metabolism to growth arrest and apoptosis.[74] We showed previously that the vitrification of embryos significantly elevates the expression level of this stress-responsive gene compared to fresh blastocysts.[75] Interestingly, using the on-chip CPA loading did not have a significant effect on the expression level of *Trp53* [Fig. 7(d)]. This can be primarily due to the fact that *Trp53* is regulated by numerous pathways during vitrification, and improvement in one of them, osmotic stress, was not sufficient to reduce its transcription level. Unlike P53, caspases are a crucial family of proteases that mediate apoptosis during its initiation and execution stages. One of the P53-activated members of the caspase family, Caspase-3, is known to act as a death protease during apoptosis execution by catalyzing the specific cleavage of multiple substrates.[76] Here, we observed that using the on-chip CPA loading significantly reduced the expression level of caspase-3 [Fig. 7(d)]. This reduced molecular footprint, which does not seem to directly correlate with *Trp53*, can be due to minimized osmotic stress in the microfluidic system and its further effect on preventing mitochondrial function impairment and preserving membrane integrity.

CONCLUSION

Here, we introduced a new microfluidic platform that allowed us to automate the CPA loading process and also push the boundaries of CPA loading by the passive introduction of the non-permeating CPA throughout the process. To the best of our knowledge, the platform introduced here is the first that can be directly followed by the cooling process, constituting a complete vitrification cycle without any additional equipment. The gradual CPA loading profile of this platform allowed shortening the total CPA loading process by 3 min with no negative impact on post-vitrification re-expansion and hatching rates. The reduced osmotic stress of this device significantly reduced the molecular impact of cryopreservation compared to those prepared with the gold standard manual method. Besides the automation, the fully standalone system described here provides a new paradigm to explore novel cryoprotective conditions (CPA composition and loading time), while remaining easy-to-use, reproducible, and amenable to high throughput and parallel workflows. We believe that the results presented here will establish microfluidic systems as an invaluable tool for cryopreservation without the hassle of commonly necessitated supporting equipment such as pumps and tubing. Moreover, the introduction of osmotic stress-free chemical loading enables a new chapter in CPA design and opens the door to new solutions that are currently deemed unsuitable because of their high osmotic pressure, toxicity over long loading cycles, or handling difficulties.

SUPPLEMENTARY MATERIAL

See Table SI in the supplementary material that contains the list of primer pairs used to amplify the genes of interest in real-time qPCR. Figure S1 shows the plot of concentration as a function of absorption of the marker dye used in validating the chip's performance. Figure S2 is the schematic representation of molecular damages studied in this work.

AUTHORS' CONTRIBUTIONS

P.T. contributed in conceptualization, investigation, methodology, writing original draft, and editing. F.S. contributed in investigation,

methodology, visualization, writing original draft, and editing. M.N. contributed in investigation, formal analysis, and data validation. P.K. contributed in conceptualization, investigation, and methodology. S.A. contributed in formal analysis, investigation, and visualization. S.F. contributed in investigation and formal analysis. G.Z., N.Z., and A.Sh.Z.N. contributed in investigation and methodology. A.E. contributed in writing original draft and editing and resources, and M.D. supervised and funded the project and contributed in writing original draft and editing.

ACKNOWLEDGMENTS

This study was supported by a grant from the National Institute of Genetic Engineering and Biotechnology (No. 677). The authors would like to thank Dr. Mehdi Fardmanesh and his group at the Sharif University of Technology for the stimulating conversations, assistance in microfabrication, and editing the manuscript. We would also like to thank Camille Cassel de Camps for her assistance in preparing the manuscript and Yuanyuan Tao for his help in image analysis.

There is no conflict to declare.

DATA AVAILABILITY

The data that support the findings of this study are available from the corresponding author upon reasonable request.

REFERENCES

[1]A. Trounson and L. Mohr, "Human pregnancy following cryopreservation, thawing and transfer of an eight-cell embryo," Nature **305**(5936), 707–709 (1983).
[2]V. A. Kushnir, D. H. Barad, D. F. Albertini, S. K. Darmon, and N. Gleicher, "Systematic review of worldwide trends in assisted reproductive technology 2004–2013," Reprod. Biol. Endocrinol. **15**(1), 6 (2017).
[3]M. J. Taylor, B. P. Weegman, S. C. Baicu, and S. E. Giwa, "New approaches to cryopreservation of cells, tissues, and organs," Transfus. Med. Hemother. **46**(3), 197–215 (2019).
[4]G. D. Elliott, S. Wang, and B. J. Fuller, "Cryoprotectants: A review of the actions and applications of cryoprotective solutes that modulate cell recovery from ultra-low temperatures," Cryobiology **76**, 74–91 (2017).
[5]H. Sieme, H. Oldenhof, and W. F. Wolkers, "Mode of action of cryoprotectants for sperm preservation," Anim. Reprod. Sci. **169**, 2–5 (2016).
[6]F. Gu, S. Li, L. Zheng, J. Gu, T. Li, H. Du *et al.*, "Perinatal outcomes of singletons following vitrification versus slow-freezing of embryos: A multicenter cohort study using propensity score analysis," Hum. Reprod. **34**(9), 1788–1798 (2019).
[7]L. Rienzi, C. Gracia, R. Maggiulli, A. R. LaBarbera, D. J. Kaser, F. M. Ubaldi *et al.*, "Oocyte, embryo and blastocyst cryopreservation in ART: Systematic review and meta-analysis comparing slow-freezing versus vitrification to produce evidence for the development of global guidance," Hum. Reprod. Update **23**(2), 139–155 (2017).
[8]K. S. Richter, D. K. Ginsburg, S. K. Shipley, J. Lim, M. J. Tucker, J. R. Graham *et al.*, "Factors associated with birth outcomes from cryopreserved blastocysts: Experience from 4,597 autologous transfers of 7,597 cryopreserved blastocysts," Fertil. Steril. **106**(2), 354–362 (2016).
[9]Z. P. Nagy, D. Shapiro, and C.-C. Chang, "Vitrification of the human embryo: A more efficient and safer in vitro fertilization treatment," Fertil. Steril. **113**(2), 241–247 (2020).
[10]A. Kresna and T. D. Lestari, "Cryoprotectant combination ethylene glycol and propanediol on mice blastocyst viability post vitrification," J. Phys.: Conf. Ser. **1146**, 012028 (2019).
[11]B. P. Best, "Cryoprotectant toxicity: Facts, issues, and questions," Rejuvenation Res. **18**(5), 422–436 (2015).
[12]J. Lu, M. Sheng, P. Yao, C. Ran, H. Liu, L. Chen *et al.*, "High concentration of glucose increases reactive oxygen species generation and apoptosis induced by endoplasmic reticulum stress pathway in rabbit corneal epithelial cells," J. Ophthalmol. **2018**, 8234906.
[13]J. I. Burgos, M. Morell, J. I. E. Mariángelo, and M. V. Petroff, "Hyperosmotic stress promotes endoplasmic reticulum stress-dependent apoptosis in adult rat cardiac myocytes," Apoptosis **24**(9-10), 785–797 (2019).
[14]S. Mullen, M. Rosenbaum, and J. Critser, "The effect of osmotic stress on the cell volume, metaphase II spindle and developmental potential of *in vitro* matured porcine oocytes," Cryobiology **54**(3), 281–289 (2007).
[15]R. Ruan, L. Zou, S. Sun, J. Liu, L. Wen, D. Gao *et al.*, "Cell blebbing upon addition of cryoprotectants: A self-protection mechanism," PloS One **10**(4), e0125746 (2015).
[16]T. Tharasanit, S. Manee-In, S. Buarpung, K. Chatdarong, C. Lohachit, and M. Techakumphu, "Successful pregnancy following transfer of feline embryos derived from vitrified immature cat oocytes using 'stepwise'cryoprotectant exposure technique," Theriogenology **76**(8), 1442–1449 (2011).
[17]G. Wu, B. Jia, G. Quan, D. Xiang, B. Zhang, Q. Shao *et al.*, "Vitrification of porcine immature oocytes: Association of equilibration manners with warming procedures, and permeating cryoprotectants effects under two temperatures," Cryobiology **75**, 21–27 (2017).
[18]K. F. Sonnen and C. A. Merten, "Microfluidics as an emerging precision tool in developmental biology," Dev. Cell **48**(3), 293–311 (2019).
[19]Y.-J. Ko, J.-H. Maeng, S. Y. Hwang, and Y. Ahn, "Design, fabrication, and testing of a microfluidic device for thermotaxis and chemotaxis assays of sperm," SLAS Technol. Transl. Life Sci. Innovation **23**(6), 507–515 (2018).
[20]S. Bhagwat, S. Sontakke, P. Parte, and S. Jadhav, "Chemotactic behavior of spermatozoa captured using a microfluidic chip," Biomicrofluidics **12**(2), 024112 (2018).
[21]R. Nosrati, P. J. Graham, B. Zhang, J. Riordon, A. Lagunov, T. G. Hannam *et al.*, "Microfluidics for sperm analysis and selection," Nat. Rev. Urol. **14**(12), 707–730 (2017).
[22]R. Samuel, H. Feng, A. Jafek, D. Despain, T. Jenkins, and B. Gale, "Microfluidic-based sperm sorting & analysis for treatment of male infertility," Transl. Androl. Urol. **7**(Suppl. 3), S336 (2018).
[23]W. Iwasaki, K. Yamanaka, D. Sugiyama, Y. Teshima, M. P. Briones-Nagata, M. Maeki *et al.*, "Simple separation of good quality bovine oocytes using a microfluidic device," Sci. Rep. **8**(1), 14273 (2018).
[24]Z. Chen, Z. Zhang, X. Guo, K. Memon, F. Panhwar, M. Wang *et al.*, "Sensing cell membrane biophysical properties for detection of high quality human oocytes," ACS Sens. **4**(1), 192–199 (2018).
[25]S. Thapa and Y. S. Heo, "Microfluidic technology for in vitro fertilization (IVF)," JMST Adv. **1**, 1–11 (2019).
[26]L. Weng, "IVF-on-a-chip: Recent advances in microfluidics technology for in vitro fertilization," SLAS Technol.: Transl. Life Sci. Innovation **24**(4), 373–385 (2019).
[27]M.-S. Lee, W. Hsu, H.-Y. Huang, H.-Y. Tseng, C.-T. Lee, C.-Y. Hsu *et al.*, "Simultaneous detection of two growth factors from human single-embryo culture medium by a bead-based digital microfluidic chip," Biosens. Bioelectron. **150**, 111851 (2020).
[28]H.-Y. Huang, H.-H. Shen, C.-H. Tien, C.-J. Li, S.-K. Fan, C.-H. Liu *et al.*, "Digital microfluidic dynamic culture of mammalian embryos on an electrowetting on dielectric (EWOD) chip," PloS One **10**(5), e0124196 (2015).
[29]S. Xiao, J. R. Coppeta, H. B. Rogers, B. C. Isenberg, J. Zhu, S. A. Olalekan *et al.*, "A microfluidic culture model of the human reproductive tract and 28-day menstrual cycle," Nat. Commun. **8**(1), 1–13 (2017).
[30]W. Zhuo, H. Lu, and P. T. McGrath, "Microfluidic platform with spatiotemporally controlled micro-environment for studying long-term *C. elegans* developmental arrests," Lab Chip **17**(10), 1826–1833 (2017).

[31]M. A. Ferraz, H. H. Henning, P. F. Costa, J. Malda, F. P. Melchels, R. Wubbolts *et al.*, "Improved bovine embryo production in an oviduct-on-a-chip system: Prevention of poly-spermic fertilization and parthenogenic activation," Lab Chip **17**(5), 905–916 (2017).
[32]J. S. Gnecco, T. Ding, C. Smith, J. Lu, K. L. Bruner-Tran, and K. G. Osteen, "Hemodynamic forces enhance decidualization via endothelial-derived prostaglandin E2 and prostacyclin in a microfluidic model of the human endometrium," Hum. Reprod. **34**(4), 702–714 (2019).
[33]Y. Baert, I. Ruetschle, W. Cools, A. Oehme, A. Lorenz, U. Marx *et al.*, "A multi-organ-chip co-culture of liver and testis equivalents: A first step toward a systemic male reprotoxicity model," Hum. Reprod. **35**(5), 1029–1044 (2020).
[34]Y. Zheng, G. Zhao, Y. Zhang, and R. Gao, "On-chip loading and unloading of cryoprotectants facilitate cell cryopreservation by rapid freezing," Sens. Actuators, B **255**, 647–656 (2018).
[35]D. G. Pyne, J. Liu, M. Abdelgawad, and Y. Sun, "Digital microfluidic processing of mammalian embryos for vitrification," PloS One **9**(9), e108128 (2014).
[36]Z. Chen, K. Memon, Y. Cao, and G. Zhao, "A microfluidic approach for synchronous and nondestructive study of the permeability of multiple oocytes," Microsyst. Nanoeng. **6**(1), 1 (2020).
[37]Y. S. Heo, H.-J. Lee, B. A. Hassell, D. Irimia, T. L. Toth, H. Elmoazzen *et al.*, "Controlled loading of cryoprotectants (CPAs) to oocyte with linear and complex CPA profiles on a microfluidic platform," Lab Chip **11**(20), 3530–3537 (2011).
[38]Z. Lei, D. Xie, M. K. Mbogba, Z. Chen, C. Tian, L. Xu *et al.*, "A microfluidic platform with cell-scale precise temperature control for simultaneous investigation of the osmotic responses of multiple oocytes," Lab Chip **19**(11), 1929–1940 (2019).
[39]M. R. Freeman, M. S. Hinds, K. G. Howard, J. M. Howard, and G. A. Hill, "Guidance for elective single-embryo transfer should be applied to frozen embryo transfer cycles," J. Assist. Reprod. Genet. **36**(5), 939–946 (2019).
[40]J. Haas, J. Meriano, C. Laskin, Y. Bentov, E. Barzilay, R. F. Casper *et al.*, "Clinical pregnancy rate following frozen embryo transfer is higher with blastocysts vitrified on day 5 than on day 6," J. Assist. Reprod. Genet. **33**(12), 1553–1557 (2016).
[41]J. Zhao, Y. Yan, X. Huang, L. Sun, and Y. Li, "Blastocoele expansion: An important parameter for predicting clinical success pregnancy after frozen-warmed blastocysts transfer," Reprod. Biol. Endocrinol. **17**(1), 15 (2019).
[42]H. Chen, C. Chen, S. Bai, Y. Gao, G. Metcalfe, W. Cheng *et al.*, "Multiplexed detection of cancer biomarkers using a microfluidic platform integrating single bead trapping and acoustic mixing techniques," Nanoscale **10**(43), 20196–20206 (2018).
[43]Z. Chen, Y. Zhu, D. Xu, M. M. Alam, L. Shui, and H. Chen, "Cell elasticity measurement using a microfluidic device with real-time pressure feedback," Lab Chip **20**(13), 2343–2353 (2020).
[44]M. Kuwayama, "Highly efficient vitrification for cryopreservation of human oocytes and embryos: The cryotop method," Theriogenology **67**(1), 73–80 (2007).
[45]B. Kovačič and V. Vlaisavljević, "Importance of blastocyst morphology in selection for transfer," in *Advances in Embryo Transfer* (IntechOpen, 2012), pp. 161–177.
[46]J. Jeon, N. Choi, H. Chen, J.-I. Moon, L. Chen, and J. Choo, "SERS-based droplet microfluidics for high-throughput gradient analysis," Lab Chip **19**(4), 674–681 (2019).
[47]N. Garcia-Seyda, L. Aoun, V. Tishkova, V. Seveau, M. Biarnes-Pelicot, M. Bajénoff *et al.*, "Microfluidic device to study flow-free chemotaxis of swimming cells," Lab Chip **20**(9), 1639–1647 (2020).
[48]B. Lee, H.-H. Jeong, K.-K. Kang, C.-S. Lee, and S.-H. Lee, "Improvement of a diffusion-based microfluidic chemotaxis assay through stable formation of a chemical gradient," Chem. Eng. Sci. **202**, 130–137 (2019).
[49]X. Zhou, Z. Jiang, X. M. Liang, J. Liu, P. Fang, Z. Liu *et al.*, "Microfiltration-based sequential perfusion: A new approach for improved loading/unloading of cryoprotectants," Sens. Actuators, B **312**, 127957 (2020).
[50]G. Zhao and J. Fu, "Microfluidics for cryopreservation," Biotechnol. Adv. **35**(2), 323–336 (2017).
[51]Y. Guo, Y. Yang, X. Yi, and X. Zhou, "Microfluidic method reduces osmotic stress injury to oocytes during cryoprotectant addition and removal processes in porcine oocytes," Cryobiology **90**, 63–70 (2019).
[52]G. Zhao, Z. Zhang, Y. Zhang, Z. Chen, D. Niu, Y. Cao *et al.*, "A microfluidic perfusion approach for on-chip characterization of the transport properties of human oocytes," Lab Chip **17**(7), 1297–1305 (2017).
[53]D. Lai, J. Ding, G. Smith, G. Smith, and S. Takayama, "Slow and steady cell shrinkage reduces osmotic stress in bovine and murine oocyte and zygote vitrification," Hum. Reprod. **30**(1), 37–45 (2015).
[54]S. Friedler, L. C. Giudice, and E. J. Lamb, "Cryopreservation of embryos and ova," Fertil. Steril. **49**(5), 743–764 (1988).
[55]A. Ampaw, T. A. Charlton, J. G. Briard, and R. N. Ben, "Designing the next generation of cryoprotectants—From proteins to small molecules," Pept. Sci. **111**(1), e24086 (2019).
[56]K. G. M. Mahmoud, M. El-Sokary, T. Scholkamy, M. Abou El-Roos, G. Sosa, and M. Nawito, "The effect of cryodevice and cryoprotectant concentration on buffalo oocytes vitrified at MII stage," Anim. Reprod. **10**(4), 689–696 (2013).
[57]N. Shardt, Z. Chen, S. C. Yuan, K. Wu, L. Laouar, N. M. Jomha *et al.*, "Using engineering models to shorten cryoprotectant loading time for the vitrification of articular cartilage," Cryobiology **92**, 180–188 (2020).
[58]G. Rabbani and I. Choi, "Roles of osmolytes in protein folding and aggregation in cells and their biotechnological applications," Int. J. Biol. Macromol. **109**, 483–491 (2018).
[59]T. Lamitina, C. G. Huang, and K. Strange, "Genome-wide RNAi screening identifies protein damage as a regulator of osmoprotective gene expression," Proc. Natl. Acad. Sci. U.S.A. **103**(32), 12173–12178 (2006).
[60]M. E. Murphy, "The HSP70 family and cancer," Carcinogenesis **34**(6), 1181–1188 (2013).
[61]Y. Zhao, Z.-H. Du, M. Talukder, J. Lin, X.-N. Li, C. Zhang *et al.*, "Crosstalk between unfolded protein response and Nrf2-mediated antioxidant defense in Di-(2-ethylhexyl) phthalate-induced renal injury in quail (*Coturnix japonica*)," Environ. Pollut. **242**, 1871–1879 (2018).
[62]P. Bozaykut, N. K. Ozer, and B. Karademir, "Regulation of protein turnover by heat shock proteins," Free Radic. Biol. Med. **77**, 195–209 (2014).
[63]H. H. Kampinga and E. A. Craig, "The HSP70 chaperone machinery: J proteins as drivers of functional specificity," Nat. Rev. Mol. Cell Biol. **11**(8), 579–592 (2010).
[64]M. Castillo-Martín, M. Yeste, E. Pericuesta, R. Morató, A. Gutiérrez-Adán, and S. Bonet, "Effects of vitrification on the expression of pluripotency, apoptotic and stress genes in *in vitro*-produced porcine blastocysts," Reprod. Fertil. Dev. **27**(7), 1072–1081 (2015).
[65]T. Lin, J. E. Lee, J. W. Kang, H. Y. Shin, J. B. Lee, and D. I. Jin, "Endoplasmic reticulum (ER) stress and unfolded protein response (UPR) in mammalian oocyte maturation and preimplantation embryo development," Int. J. Mol. Sci. **20**(2), 409 (2019).
[66]A. Almanza, A. Carlesso, C. Chintha, S. Creedican, D. Doultsinos, B. Leuzzi *et al.*, "Endoplasmic reticulum stress signalling–from basic mechanisms to clinical applications," FEBS J. **286**(2), 241–278 (2019).
[67]C. Hetz, K. Zhang, and R. J. Kaufman, "Mechanisms, regulation and functions of the unfolded protein response," Nat. Rev. Mol. Cell Biol. **21**, 421–438 (2020).
[68]N. Chaudhari, P. Talwar, A. Parimisetty, C. Lefebvre d'Hellencourt, and P. Ravanan, "A molecular web: Endoplasmic reticulum stress, inflammation, and oxidative stress," Front. Cell. Neurosci. **8**, 213 (2014).
[69]H. M. A. Zeeshan, G. H. Lee, H.-R. Kim, and H.-J. Chae, "Endoplasmic reticulum stress and associated ROS," Int. J. Mol. Sci. **17**(3), 327 (2016).

[70]J. S. Len, W. S. D. Koh, and S.-X. Tan, "The roles of reactive oxygen species and antioxidants in cryopreservation," Biosci. Rep. **39**(8), BSR20191601 (2019).
[71]Y. Wang, R. Branicky, A. Noë, and S. Hekimi, "Superoxide dismutases: Dual roles in controlling ROS damage and regulating ROS signaling," J. Cell Biol. **217**(6), 1915–1928 (2018).
[72]H. Men, R. L. Monson, J. J. Parrish, and J. J. Rutledge, "Degeneration of cryopreserved bovine oocytes via apoptosis during subsequent culture," Cryobiology **47**(1), 73–81 (2003).
[73]C. Wang and R. J. Youle, "The role of mitochondria in apoptosis," Annu. Rev. Genet. **43**, 95–118 (2009).
[74]K. D. Sullivan, M. D. Galbraith, Z. Andrysik, and J. M. Espinosa, "Mechanisms of transcriptional regulation by p53," Cell Death Differ. **25**(1), 133–143 (2018).
[75]F. Sarmadi, P. Kazemi, P. Tirgar, S. Fayazi, S. Esfandiari, L. Sotoodeh *et al.*, "Using natural honey as an anti-oxidant and thermodynamically efficient cryoprotectant in embryo vitrification," Cryobiology **91**, 30–39 (2019).
[76]A. G. Porter and R. U. Jänicke, "Emerging roles of caspase-3 in apoptosis," Cell Death Differ. **6**(2), 99–104 (1999).